Journal Name

Dynamic Article Links ►

Cite this: DOI: 10.1039/c0xx00000x

www.rsc.org/xxxxxx

ARTICLE TYPE

# Atomistic modeling of site exchange defects in lithium iron phosphate and iron phosphate

*Christian Kuss,[a] Guoxian Liang,[b] Steen B. Schougaard*[a]*

***Received (in XXX, XXX) Xth XXXXXXXXX 20XX, Accepted Xth XXXXXXXXX 20XX***

**DOI: 10.1039/b000000x**

A new set of potentials is presented that allows for modeling of the entire lithium insertion range of the lithium iron phosphate system ($Li_xFePO_4$, $0 \leq x \leq 1$). By comparing calculated values to experimental crystallographic, spectroscopic and thermodynamic data, the potentials ability to reproduce experimental results consistently and reliably is demonstrated. Calculations of site exchange defect thermodynamics and diffusion barriers for lithium and iron inside the lithium diffusion path suggest that site exchange defect related capacity loss may be justified exclusively by thermodynamic considerations. Moreover, a low activation barrier for iron transport in the lithium diffusion channel in $FePO_4$ brings into question the significance of the antisite iron ion as an obstacle to lithium diffusion.

## Introduction

In recent years, interest in the global climate crisis has been rising. This interest and the belief that the limits of global fossil fuel resources exploitation are imminent[1] have boosted the search for alternative energy sources and storage devices. Hence, lithium ion batteries are being developed on a massive scale for applications ranging from electric transportation to storage facilities buffering the energy needs of whole communities.[2] One very promising positive electrode material for medium to large lithium ion batteries is lithium iron phosphate ($LiFePO_4$),[3] as it is produced from low cost, non-toxic raw materials, is stable[4] and achieves relatively high charge storage capacities with the theoretical limit of 170 mAh/g. [3]

Many different synthesis routes have been developed to produce what is nominally *olivine*-$LiFePO_4$,[1-5] however, the material exhibits significant performance differences depending on its preparation route.[5] To achieve consistently the best possible product, it is therefore essential to understand the mechanisms behind these performance fluctuations. To this end material modeling plays a crucial role as a compliment to nanoscale characterization techniques like TEM *etc*.[6-9]

Several modeling techniques have already been exploited to investigate $LiFePO_4$ batteries at different levels spanning from atomistic to macroscopic scales. At the atomic scale, *ab initio*[10-15], as well as empirical[16-18] techniques have been employed to study $LiFePO_4$. Investigation of the $Li_xFePO_4$ system has been conducted very thoroughly using the computationally expensive first principles methods.[10, 11, 15, 19] Yet, approaching some of the system's central issues, such as defect chemistry and interface dynamics,[20] these techniques quickly reach the available resource limits. Alternatively, using empirical techniques, as is the case in the present paper, makes it possible to investigate problems that require a several orders of magnitudes larger number of atoms to capture the central properties.

Most widely available empirical modeling software for ionic solids are based on calculations employing a set of interatomic empirical potentials. In the case of the $LiFePO_4$ system a set of potential parameters has previously been derived, however, for use exclusively with *fully* lithiated $LiFePO_4$.[16] Other studies use a more general set of potentials, entailing a loss in specificity of the applied assumptions of the model.[17] By means of atomistic modeling, site exchange defects have been determined to exhibit a low defect energy.[16] Consequent investigation of antisite and site exchange defects led to the direct observation and quantification of these defects and the study of their effect on the materials performance.[8, 21, 22] Depending on the preparation route site exchange defects can occur in concentrations up to 8%.[21]

To investigate the whole compositional range of the $Li_xFePO_4$ system ($0 \leq x \leq 1$), a new set of potential parameters is presented here that covers the various iron oxidation states. Moreover, in a first application of this new set of potentials, we study the importance of thermodynamics in the lithium extraction process of $LiFePO_4$ with site exchange defects, as well as, lithium and iron ion mobility in the lithium diffusion channel of these materials.

## Methods

### Model and interatomic potentials

The modeled systems were represented by a group of point ions, signifying the ionic constituents of the real material and by interactions between these elements through empirical potential functions. The well-established General Utility Lattice Program (GULP) code by J.D. Gale was used for all presented calculations. It has been extensively reviewed elsewhere.[23] The empirical potential method works particularly well for purely ionic systems, but can also be employed successfully for mixed ionic and covalent substances such as $LiFePO_4$.[16, 18, 24] In this study, long range

interactions, were modeled by simple Coulomb interaction, whereas short range repulsive and van der Waals interactions took on the form of the Buckingham potential.[25] These Buckingham pair potentials were applied for Li−O, Fe(II)−O, Fe(III)−O, P−O and O−O interactions. A shell model, binding a charged massless shell to the point ion of the core with a harmonic spring model,[26] was employed for the polarizable oxygen ions.

As the potential parameters are dependent on the system being modeled, they have been fitted extensively to the experimentally found crystal structures of pure *olivine* $LiFePO_4$ and pure *heterosite* $FePO_4$ (see reference 23 for a detailed account of the fitting procedure). In an advanced stage of the fitting process, the strongest vibrational frequency from the *heterosite* $FePO_4$ infrared spectrum was included as an observable. The final optimized parameters are summarized in Table 1.

For the calculation of intermediate compositions $Li_xFePO_4$, primitive unit cells were created in which lithium defects were placed in different orderings. After geometry optimization the most stable configuration was chosen for further calculations. Intermediate oxidation states of iron, required for solid solution calculations, were treated using a mean field approach. The iron sites were thereby assumed to be partially occupied by Fe(II) and Fe(III) at the same time, while their interactions were scaled by the appropriate factor. The vibrational energies and infrared activities of Gamma point phonon modes have been calculated from single point vibrational calculations of the relaxed structures.

**Defect calculations**

For site exchange defect calculations, 50 super cells of 48 formula units each, containing randomly distributed site exchange defects for 1/12 or 1/24 of all crystallographic lithium and iron sites (corresponding to approximately 8% and 4% site exchange defects respectively) were used. Free energies of defects were obtained from single point vibrational calculations at the 0 K optimized structure with a Monkhorst-Pack grid of 2x2x2 k-points, where free energies were converged to 0.04 eV (at the chosen super cell size). No statistically significant change in the defect energies were observed when reducing the super cell size. Cited statistical errors are based on a 95 % confidence interval for a two-tailed Student distribution.

Table 1. Potential parameters

| | Buckingham potential parameters | | |
|---|---|---|---|
| Interaction | A / eV | ρ / Å | C / eV · Å$^6$ |
| $Li^+$–$O^{2-}$ | 381.5244 | 0.30491 | 0 |
| $Fe^{2+}$–$O^{2-}$ | 13207.008 | 0.22245 | 0 |
| $Fe^{3+}$–$O^{2-}$ | 2111.9671 | 0.28941 | 0 |
| $P^{5+}$–$O^{2-}$ | 1028.9741 | 0.33530 | 0 |
| $O^{2-}$–$O^{2-}$ | 39.7594 | 0.47713 | 53.204 |
| Species | Core charge | Shell charge | $k_S$ / eV/Å$^2$ |
| $Li^+$ | +1 | – | – |
| $Fe^{2+}$ | +2 | – | – |
| $Fe^{3+}$ | +3 | – | – |
| $P^{5+}$ | +4.9708 | – | – |
| $O^{2-}$ | +0.9015 | −2.8942 | 67.3564 |

**Diffusion calculations**

The ion diffusion activation barriers were calculated using the Mott-Littleton approach[27] as implemented in the GULP code[23] with a region 1 size of 14 Å and a region 2 size of 24 Å. Diffusion paths were obtained by displacing the moving ion along the *b*-axis and allowing relaxation in *a* and *c* crystallographic directions only. Diffusion coefficients have been estimated for room temperature using the Einstein-Smoluchovski equation. Perfectly anisotropic diffusion along the b-axis and an attempt frequency of $1.4 \cdot 10^{13}$ Hz was assumed. This frequency was derived from the phonon mode with strongest lithium movement along the *b*-axis in $LiFePO_4$. As the oxidation state of antisite iron ions is not known, the activation barrier for iron ion diffusion was calculated with the extreme values of the oxidation state, i.e. +2 and +3.

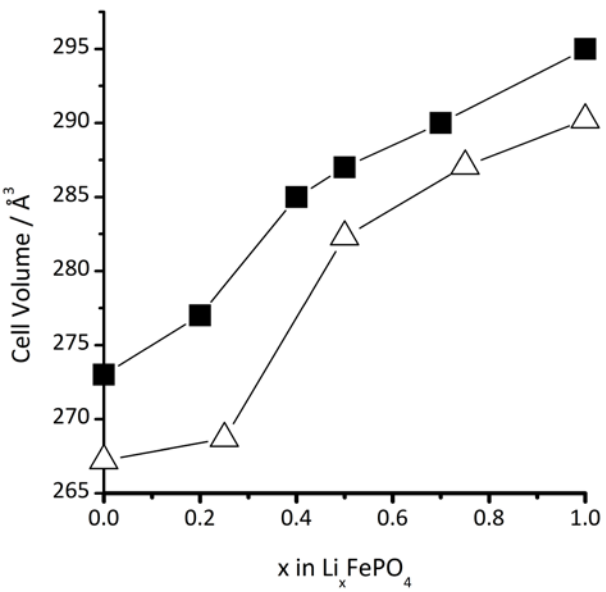


Figure 1. Experimental (solid squares, by Delacourt *et al.*[28]) and calculated (open triangles) cell volume as a function of composition in the solid solution $Li_xFePO_4$.

## Results and Discussion

**Potential validation**

The crystal structure of both end members of the $Li_xFePO_4$ system is very well reproduced by the model (Table 2) with relative errors for crystal structure parameters within 0.5 %. The same general agreement can be found when comparing the calculated dielectric constant of $LiFePO_4$ to earlier results (electronic supplementary information). Properties and crystal structures of intermediate compositions $Li_xFePO_4$ have also been calculated. $Li_xFePO_4$ equilibrates into a two phase system under ambient conditions. However, when heating the phase separated material, a solid solution behavior can be observed.[28] As shown in Figure 1 the experimentally found unit cell volume compares well to the calculated ones. Since the interatomic potentials have been fitted to ambient condition structures while the experiment is conducted at 350°C the calculated unit cell is slightly smaller. Transferability of the potentials to other structures of composition $Li_xFe_yPO_4$

Table 2. Reproduction of experimental crystal structures

| $LiFePO_4$ | Calculated | Experimental[29] | Δ / % |
|---|---|---|---|
| a / Å | 10.362 | 10.338 | + 0.2 |
| b / Å | 5.983 | 6.011 | − 0.5 |
| c / Å | 4.680 | 4.695 | − 0.3 |
| $FePO_4$ | | | |
| a / Å | 9.763 | 9.760 | + 0.04 |
| b / Å | 5.740 | 5.752 | − 0.2 |
| c / Å | 4.767 | 4.756 | + 0.2 |

($2y \leq 3\text{-}x \leq 3y$) is presented in the electronic supplementary information.

Crystal structures serve to evaluate a model's ability to predict local minima in the potential energy surface. However, in order to calculate most properties accurately, the curvature of the potential energy surface needs to be reproduced as well. To this end, tests of the reproduction of vibrational energies using infrared spectroscopic results showed strong correlation between calculation and experiment (Figure 2).

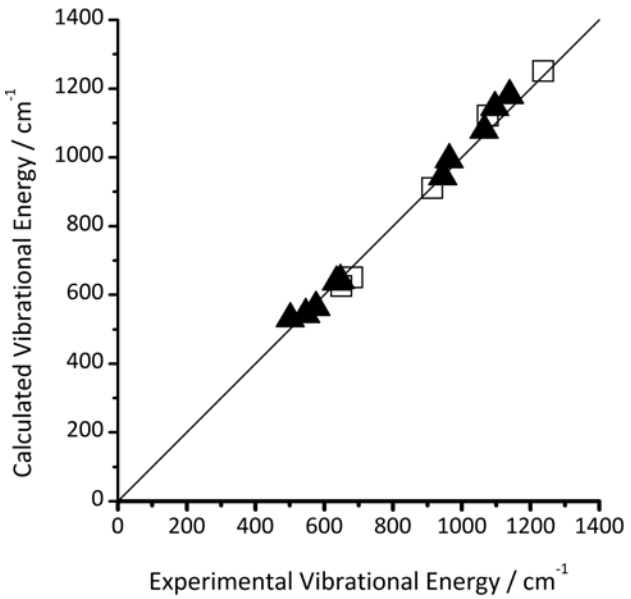


Figure 2. Correlation between calculated and experimental vibrational energies derived from infrared spectroscopy for $LiFePO_4$[30] (solid triangles) and for $FePO_4$[31] (open squares). Black line: Perfect correlation.

**Lithium diffusion in FePO4 and LiFePO4**

*Olivine* $LiFePO_4$, as well as, *heterosite* $FePO_4$ crystalize in the *Pnma* space-group. Lithium and iron thereby occupy 4a and 4c Wyckoff positions respectively. In the following, the abbreviation M1 for the crystallographic lithium site and M2 for the crystallographic iron site will be used. The mechanism of lithium motion in the $Li_xFePO_4$ system during battery operation is a subject of intense research and discussion, as such it is not yet clear if lithium moves through a lithium rich phase, a lithium poor phase, an interphase or in a solid solution.[6, 32, 33] However, it is generally accepted that lithium moves preferably along the *b* crystallographic direction.[16, 34, 35] We therefore apply the technique employed by Islam *et al.* to compare the movement of lithium ions in $FePO_4$ and $LiFePO_4$ within our model.[16] The activation barrier for a lithium ion to move from one M1 site to

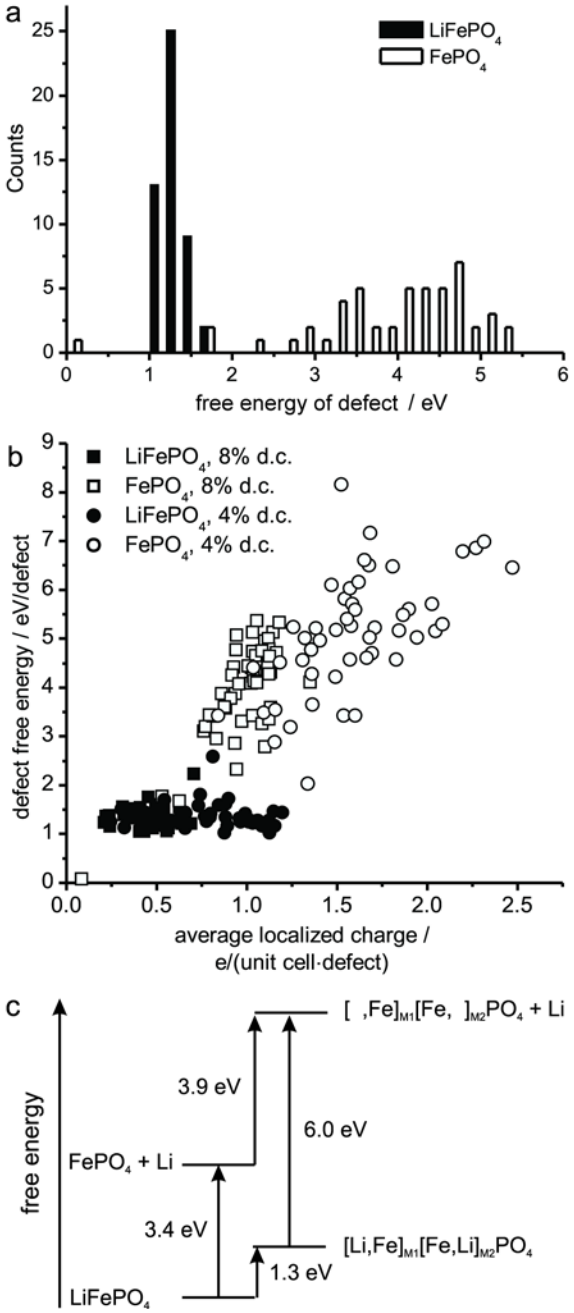


Figure 3. a) Histograms showing the distribution of free energies of defects in $LiFePO_4$ (solid bars) and $FePO_4$ (open bars) among 50 Super Cells with 8% site exchange defect concentration. b) Correlation of free energy of defects with average local charge in $LiFePO_4$ (solid symbols) and $FePO_4$ (open symbols) at 8% defect concentration (squares) and 4% defect concentration (circles). c) Illustration of average site exchange defect energies in $LiFePO_4$ and $FePO_4$ and the consequence for electrochemical cycling.

the next along the *b*-axis was calculated to 0.415 eV in $FePO_4$ and 0.420 eV in $LiFePO_4$. Based on these values, the estimated lithium diffusion coefficient is $5 \cdot 10^{-10}$ $cm^2/s$ in both $FePO_4$ and $LiFePO_4$. Moreover, investigating the diffusion path, little difference can be found between lithium diffusion in $LiFePO_4$ and $FePO_4$. It follows a curved trajectory, in order to maximize the distance to the

positively charged iron ions. This is consistent with previously reported models.[7, 16] It has been suggested before that electron transport has a significant impact on ion diffusion barriers in the $Li_xFePO_4$ system.[7, 19] Nevertheless, the comparably good agreement of our calculations, which does not invoke electronic transport, with the experimental values of $10^{-11}$ - $10^{-17}$ $cm^2/s$ is noteworthy.[36]

**Thermodynamics of delithiation of site exchange defects**

Defects have frequently been used to explain the discrepancy between calculated and observed diffusion coefficients.[7, 37] Particularly, site exchange defects are a frequent finding, whereby a lithium ion is found in a M2 site, while an iron ion is found in the M1 site.[8, 21, 22] The concentration of these defects may reach levels of more than 8%.[21] At these concentrations, correlation between defects can have a significant impact on defect energies. We therefore investigated 50 super cells with 4 or 2 randomly distributed site exchange defects each (corresponding to approx. 8 % and 4 % defect concentration respectively). Figure 3a illustrates the significant differences in defect energy and in width of energy distribution for $LiFePO_4$ and $FePO_4$ at 8% defect concentration. Free energies of defects in $LiFePO_4$ average to 1.3 eV, compared to 0.7 eV defect energy modeled by Fisher and Islam,[13, 20] while an average of 3.9 eV was found in $FePO_4$. Furthermore, correlations between the average defect energy and the position of the defects relative to each other were investigated. No statistically significant correlation could be observed in $LiFePO_4$ or $FePO_4$ with respect to average distance between point defects. However, the point defects are generally charged and as such the defect energy will likely depend on the local accumulation of charges. To assess this accumulation, a quantity was derived that we termed average localized charge. This value is calculated through integration of all charges within the volume of one unit cell, which is transposed across the relaxed super cell in ¼ unit cell length steps to obtain an average charge (Figure S1). The average localized charge is therefore zero in a theoretically perfect crystal. In general we found that super cells that exhibit a larger localized charge, also exhibit larger defect energy. In addition this effect is correlated to the material lithiation state. As a point defect in $FePO_4$ (± 3e) is more highly charged than in $LiFePO_4$ (± 1e), generally, the average localized charge also increases. Defects in $FePO_4$ therefore have more significant long range effects compared to $LiFePO_4$. This difference in range of interaction provides an explanation for the strong energy difference observed between site exchange defects in $LiFePO_4$ and in $FePO_4$ (Figure 3b). The increase of defect charge during oxidation of iron and removal of lithium from the structure leads to a strong increase in defect energy. Especially empty M2 sites are highly unstable. Transferring this to the electrochemical charging process, it is possible to calculate an additional potential necessary to fully oxidize $LiFePO_4$ containing site exchange defects.

From the reaction free energy of

$$[Li_{1-\varepsilon},Fe_\varepsilon]_{M1}[Fe_{1-\varepsilon},Li_\varepsilon]_{M2}PO_4 + [\ ]_{M1}[Fe]_{M2}PO_4 \rightarrow [Fe_\varepsilon]_{M1}[Fe_{1-\varepsilon}]_{M2}PO_4 + [Li]_{M1}[Fe]_{M2}PO_4 \quad [1]$$

this additional potential is estimated to 2.6 eV ± 0.5 eV at 25 °C (Figure 3 c), *i.e.* the potential *vs.* $Li/Li^+$ required to remove lithium from the antisite defects is 6.0 V. Electrolyte stability dictates an oxidation potential no larger than ~5V *vs.* $Li/Li^+$ for most lithium ion batteries.[38] Consequently, in the absence of a concerted exchange of the defect lithium ion by another positively charged ion, this lithium is inaccessible to electrochemical cycling (Figure 4).

Even before removing the antisite lithium, oxidation of iron and removal of lithium ions will increase defect charge. Considering the aforementioned dependence of the defect energy on defect charge, a slight increase in the lithiation and delithiation potential relative to $Li/Li^+$ is therefore expected in the presence of site exchange defects.

Recent computational studies describe the kinetic hindrance of delithiation by the presence of iron in the lithium diffusion channel.[7, 37] It was concluded that this hindrance is large and decreases the diffusion rate by several orders of magnitude compared to the theoretical perfectly crystalline $LiFePO_4$. Even the slowest estimates by Malik *et al.*, however, allow lithium transport through a 1 µm particle within approximately 15 minutes. Nevertheless, a capacity loss of the order of the site exchange defect concentration has been observed experimentally in nano-sized particles after 30 minutes delithiation time.[22] The present study suggests that this capacity loss is thermodynamic, *i.e.* permanent.

**Fe diffusion in $LiFePO_4$ and $FePO_4$**

In the above mentioned computational studies iron was regarded as immobile in the M1 site. To the best of our knowledge this assumption has not yet been proven experimentally and can rapidly be tested using the new set of potentials. To this end, the mobility of iron ions in the M1 site along the *b*-axis in $LiFePO_4$ and in $FePO_4$ has been examined. With a transport barrier of 1.2 eV, the assumption holds true for $LiFePO_4$. However, in $FePO_4$, a low diffusion barrier of only 0.45 eV to 0.50 eV is observed. Iron in the M1 site in $FePO_4$ therefore exhibits a mobility that is comparable to lithium. The migration path in both cases resembles closely the path observed for the lithium ion, with a slightly larger deviation from the linear path. In turn this puts into question the ability of iron in the M1 site to block the diffusion of the lithium, as it can move to the particle surface where its behavior is difficult to predict, but could include, dissolution into the electrolyte, inclusion in the carbon coating or displacement into a surface defect site. This would lead to an increase in capacity during the first discharge/charge cycles as has been observed by several groups.[2, 39]

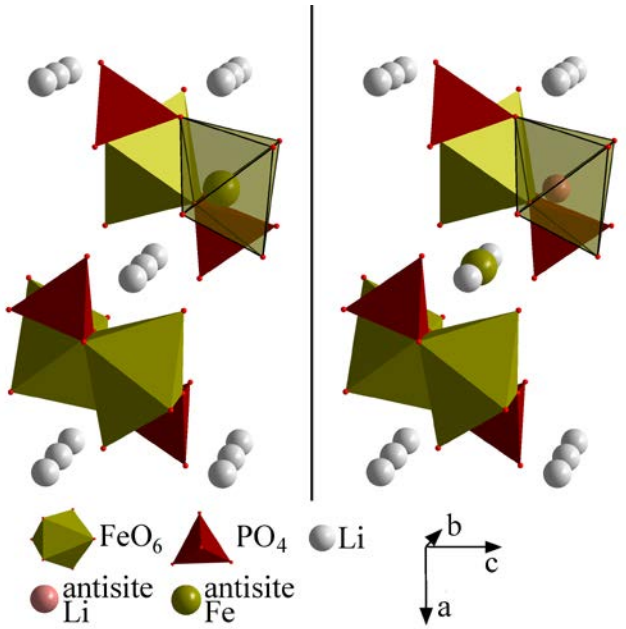


Figure 4. The site exchange defect. Left: crystalline *Pnma* $LiFePO_4$, Right: *Pnma* $LiFePO_4$ with site exchange. The lithium ion, which is hindered from delithiation, is tinted red.

## Conclusions

The presented set of potentials is a simple new tool to access accurate mechanical atomistic data across the complete composition range $Li_xFePO_4$ ($0 \leq x \leq 1$). Its estimate of the lithium diffusion barrier produces diffusion coefficients that are consistent with experimental values.

While probing the site exchange defect, a strong dependence of the defect energy on defect charge is observed. As the charge of the site exchange defect increases during delithitation, an increase in the systems energy has been predicted. This increase was quantified and is especially substantial when removing antisite lithium and leaving an empty M2 site, making this lithium inaccessible to electrochemical cycling in common batteries. Together with calculations predicting high mobility of antisite iron in the iron phosphate lithium diffusion channel, these findings challenge the current view on the mechanism of battery performance depression due to site exchange defects.

## Acknowledgements

The authors acknowledge gratefully Compute Canada's CLUMEQ for providing computational resources for this project and the National Science and Engineering Research Council of Canada (NSERC), Grant no. CRD 385812-09 for financial support. We furthermore thank Dr. S. Islam for assistance and Dr. R. Cornut for helpful discussions.

## Notes and references

[a] *Department for Chemistry, Université du Québec à Montréal, 2101 rue Jeanne-Mance, Montreal (QC) H1X 2J6, Canada*
[b] *Phostech Lithium Inc., 1475 rue Marie-Victorin, St.Bruno de Montarville (QC) J3V 6B7, Canada*

† Electronic Supplementary Information (ESI) available: Calculated mechanical properties, dielectric constants and heat capacities of $LiFePO_4$ and $FePO_4$, illustration of the average localized charge determination and transferability of the interatomic potentials. See DOI: 10.1039/b000000x/

1. T.-H. Cho and H.-T. Chung, J. Power Sources, 2004, 133, 272-276.
2. V. Palomares, A. Goñi, I. G. d. Muro, I. de Meatza, M. Bengoechea, O. Miguel and T. Rojo, J. Power Sources, 2007, 171, 879-885.
3. G. Arnold, J. Garche, R. Hemmer, S. Ströbele, C. Vogler and M. Wohlfahrt-Mehrens, J. Power Sources, 2003, 119-121, 247-251.
4. S. Yang, P. Y. Zavalij and M. S. Whittingham, Electrochem. Commun., 2001, 3, 505-508.
5. S. Franger, F. Le Cras, C. Bourbon and H. Rouault, J. Power Sources, 2003, 119-121, 252-257.
6. C. Delmas, M. Maccario, L. Croguennec, F. Le Cras and F. Weill, Nat. Mater., 2008, 7, 665-671.
7. G. K. P. Dathar, D. Sheppard, K. J. Stevenson and G. Henkelman, Chem. Mater., 2011, 23, 4032-4037.
8. S.-Y. Chung, S.-Y. Choi, T. Yamamoto and Y. Ikuhara, Phys. Rev. Lett., 2008, 100, 125502.
9. C. A. J. Fisher, V. M. Hart Prieto and M. S. Islam, Chem. Mater., 2008, 20, 5907-5915.
10. F. Zhou, T. Maxisch and G. Ceder, Phys. Rev. Lett., 2006, 97, 155704.
11. S. P. Ong, L. Wang, B. Kang and G. Ceder, Chem. Mater., 2008, 20, 1798-1807.
12. S. P. Ong, A. Jain, G. Hautier, B. Kang and G. Ceder, Electrochem. Commun., 2010, 12, 427-430.
13. X. Hou, S. Hu, W. Li, L. Zhao, Q. Ru, H. Yu and Z. Huang, Chin. Sci. Bull., 2008, 53, 1763-1767.
14. Z. Wang, S. Sun, D. Xia, W. Chu, S. Zhang and Z. Wu, J. Phys. Chem. C, 2008, 112, 17450-17455.
15. C. Ouyang, S. Shi, Z. Wang, X. Huang and L. Chen, Phys. Rev. B, 2004, 69, 104303.
16. M. S. Islam, D. J. Driscoll, C. A. J. Fisher and P. R. Slater, Chem. Mater., 2005, 17, 5085-5092.
17. S. Adams and R. P. Rao, Solid State Ionics, 2011, 184, 57-61.
18. G. R. Gardiner and M. S. Islam, Chem. Mater., 2010, 22, 1242-1248.
19. S. P. Ong, V. L. Chevrier and G. Ceder, Phys. Rev. B, 2011, 83, 075112.
20. L.-X. Yuan, Z.-H. Wang, W.-X. Zhang, X.-L. Hu, J.-T. Chen, Y.-H. Huang and J. B. Goodenough, Energy & Environmental Science, 2011, 4, 269-284.
21. J. Chen and J. Graetz, ACS Appl. Mater. Interfaces, 2011, 3, 1380-1384.
22. S.-P. Badi, M. Wagemaker, B. L. Ellis, D. P. Singh, W. J. H. Borghols, W. H. Kan, D. H. Ryan, F. M. Mulder and L. F. Nazar, J. Mater. Chem., 2011, 21, 10085-10093.
23. J. D. Gale and A. L. Rohl, Mol. Simul., 2003, 29, 291-341.
24. S. Girard, J. D. Gale, C. Mellot-Draznieks and G. Férey, Chem. Mater., 2001, 13, 1732-1738.
25. R. A. Buckingham, Proc. R. Soc. London, A, 1938, 168, 264-283.
26. B. G. Dick and A. W. Overhauser, Phys. Rev., 1958, 112, 90.
27. N. F. Mott and M. J. Littleton, Trans. Faraday Soc., 1938, 34, 485-499.
28. C. Delacourt, P. Poizot, J.-M. Tarascon and C. Masquelier, Nat. Mater., 2005, 4, 254-260.
29. G. Rousse, J. Rodriguez-Carvajal, S. Patoux and C. Masquelier, Chem. Mater., 2003, 15, 4082-4090.
30. C. M. Burba and R. Frech, J. Electrochem. Soc., 2004, 151, A1032-A1038.
31. N. D. Trinh, G. Liang, M. Gauthier and S. B. Schougaard, J. Power Sources, 2012, 200, 92-97.
32. R. Malik, F. Zhou and G. Ceder, Nat. Mater., 2011, 10, 587-590.
33. P. P. Prosini, J. Electrochem. Soc., 2005, 152, A1925-A1929.
34. J. Li, W. Yao, S. Martin and D. Vaknin, Solid State Ionics, 2008, 179, 2016-2019.
35. P. Zhang, Y. Wu, D. Zhang, Q. Xu, J. Liu, X. Ren, Z. Luo, M. Wang and W. Hong, J. Phys. Chem. A, 2008, 112, 5406-5410.
36. M. Park, X. Zhang, M. Chung, G. B. Less and A. M. Sastry, J. Power Sources, 2010, 195, 7904-7929.
37. R. Malik, D. Burch, M. Bazant and G. Ceder, Nano Lett., 2010, 10, 4123-4127.
38. K. Xu, Chem. Rev. (Washington, DC, U. S.), 2004, 104, 4303-4418.

39. J. Morales, R. Trócoli, S. Franger and J. Santos-Peña, Electrochim. Acta, 2010, 55, 3075-3082.

 